
01 May 1993

120keV Ar⁸⁺-Li Collisions Studied By Near UV And Visible Photon Spectroscopy

E. Jacquet


P. Boduch

M. Chantepie

M. Druetta

et. al. For a complete list of authors, see https://scholarsmine.mst.edu/phys_facwork/2581

Follow this and additional works at: https://scholarsmine.mst.edu/phys_facwork

 Part of the [Physics Commons](#)

Recommended Citation

E. Jacquet and P. Boduch and M. Chantepie and M. Druetta and D. Hennecart and X. Husson and D. Lecler and R. E. Olson and J. Pascale and N. Stolterfoht and M. Wilson, "120keV Ar⁸⁺-Li Collisions Studied By Near UV And Visible Photon Spectroscopy," *Physica Scripta*, vol. 47, no. 5, pp. 618 - 627, IOP Publishing; Royal Swedish Academy of Sciences, May 1993.

The definitive version is available at <https://doi.org/10.1088/0031-8949/47/5/003>

This Article - Journal is brought to you for free and open access by Scholars' Mine. It has been accepted for inclusion in Physics Faculty Research & Creative Works by an authorized administrator of Scholars' Mine. This work is protected by U. S. Copyright Law. Unauthorized use including reproduction for redistribution requires the permission of the copyright holder. For more information, please contact scholarsmine@mst.edu.

120 keV Ar⁸⁺-Li collisions studied by near UV and visible photon spectroscopy

To cite this article: E Jacquet *et al* 1993 *Phys. Scr.* **47** 618

View the [article online](#) for updates and enhancements.

You may also like

- [Identification of *Vibrio* spp. causing vibriosis in spiny lobsters \(*Panulirus homarus* L.\) in Bengkulu marine temporary shelter ponds](#)
R H Wibowo, Sipriyadi, W Darwis et al.
- [Multi-wavelength Properties of Radio- and Machine-learning-identified Counterparts to Submillimeter Sources in S2COSMOS](#)
Fang Xia An, J. M. Simpson, Ian Smail et al.
- [Metal-poor Stars Observed with the Southern African Large Telescope II. An Extended Sample](#)
Joseph Zepeda, Kaitlin C. Rasmussen, Timothy C. Beers et al.

120 keV Ar⁸⁺–Li Collisions Studied by Near UV and Visible Photon Spectroscopy

E. Jacquet,¹ P. Boduch,¹ M. Chantepie,¹ M. Druetta,² D. Hennecart,¹ X. Husson,¹ D. Lecler,¹ R. E. Olson,³ J. Pascale,⁴ N. Stolterfoht^{1,6} and M. Wilson⁵

¹ Laboratoire de spectroscopie atomique, CNRS-URA 19, ISMRA, Bd du Maréchal Juin, 14050 Caen Cedex, France

² Laboratoire de traitement du signal et instrumentation, Université de Saint-Etienne, CNRS-URA 842, 23 rue du Docteur Paul Michelon, 42023 Saint-Etienne Cedex, France

³ Department of Physics, University of Missouri–Rolla, Rolla, Missouri 65401, U.S.A.

⁴ Services des Photons, Atomes et Molécules, Centre d'Etudes de Saclay CEA, 91191 Gif Sur Yvette Cedex, France

⁵ Department of Physics, Royal Holloway University of London, Egham Hill, Egham, Surrey TW20 0EX, U.K.

⁶ Hahn-Meitner-Institut, Glienicke Strasse 100, D-1000 Berlin 39, Germany

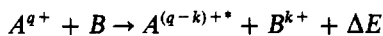
Received July 2, 1992; accepted in revised form February 11, 1993

Abstract

A spectroscopic analysis of light emitted in the 200–600 nm wavelength range by Ar⁷⁺, Ar⁶⁺ and Ar⁵⁺ ions after charge exchange in 120 keV Ar⁸⁺–Li collisions is performed. Transitions with $\Delta n = 1$ and $\Delta n = 2$ for $n = 8, 9, 10$ and 11 states of Ar VIII following single electron capture are identified and the production cross sections for $n = 8$ and $n = 9$ are deduced from emission cross sections and compared with those calculated by the three-body classical trajectory Monte-Carlo method. Lines due to double capture process were observed and identified as Rydberg transitions $3snl-3sn'l'$ ($n = 7, 8$ and 9) in Ar VII. Lines due to triple electron capture process were found and identified as transitions $3s^2nl-3s^2n'l'$ and $3s3pnl-3s3pn'l'$ ($n = 7, 8$) in Ar VI. The configurations produced during the collision provides evidence that electron–electron interaction play an important role in double and triple charge exchange processes.

1. Introduction

Electron capture by slow multiply charged ions has been the subject of intensive experimental and theoretical studies recently mainly due to the interest for applications to astrophysics [1], X-ray and UV lasers [2] and fusion plasma [3]. Collisions of multiply charged ions on a neutral atomic or molecular target produce excited multiply charged ions following the reaction:



where k is the number of electrons which have been captured.

Following previous work (Ar⁸⁺–He, Ar⁸⁺–H₂) [4, 5], we present results for collisions between Ar⁸⁺ ions and lithium atoms at 120 keV which have never been studied before. The electronic structure of the target involves specific features which makes it interesting to study single, double and triple electron transfers. First, the outer 2s electron is weakly bound and population of relatively high Rydberg states is therefore expected in Ar VIII. Such a situation has already been observed by Martin *et al.* [6] with a caesium target, but the ℓ selectivity is not yet well understood and constitutes an open field of investigations. Secondly, during the double and triple electron captures, the 2s and one or two 1s electrons are transferred. Photon spectroscopy allows one to observe radiative states populated by single, double and triple electron captures. The relative populations of the outgoing collision channels allow an estimate of the importance of correlation effects (electron–electron interactions) in the exchange processes.

Single-electron capture from a Li target has already been observed. Dijkkamp *et al.* [7] measured absolute emission cross sections of lines of the C IV spectrum in the wavelength 20–500 nm resulting from C⁴⁺–Li collisions. From these emission cross sections, they deduced one-electron transfer cross sections for $n < 8$ using known transition probabilities. Wolfrum *et al.* [8] studied Ne^{q+} ($q = 6, \dots, 9$) and C⁶⁺–Li collisions, they measured absolute visible light emission cross sections for the different $n\ell$ states produced. The distribution over ℓ within a given n shell is not found as a statistical distribution. Recent works [9, 10] have shown the validity of the three-body Monte-Carlo (CTMC) method to predict such distributions for collisions between multiply charged ions and alkali metal atom targets.

We studied Ar⁸⁺–Li collisions by photon spectroscopy in the near UV and visible wavelength range (200–600 nm). This range has been chosen because the wavelengths of a large number of lines emitted by the predicted radiative states produced are between 200 and 600 nm.

After a description of the experimental set-up, we present a detailed spectroscopic analysis of the recorded spectra. For lines due to single, double and triple electron captures, this analysis is made using collisional models (Niehaus [11]), by taking into account electron–electron interactions (Stolterfoht *et al.* [12, 13], Bachau *et al.* [14]), using spectroscopic *ab initio* pseudo-relativistic Hartree–Fock (HFR) calculations (Cowan [15]) and previous experimental data [5, 6, 16–18]. Calculations of the one-electron capture cross sections into specific n, ℓ subshells using the CTMC method [19, 20] and model potentials to describe the interactions between the electrons and the ionic cores Ar⁸⁺ and Li⁺ will also be presented and compared with experimental results.

2. Experimental set-up

A beam of 120 keV Ar⁸⁺ ions was produced by an ECR ion source at the GANIL* test bench. The Ar⁸⁺ ions are either in their ground state $1s^22s^22p^6$ (¹S₀) or in the metastable state $1s^22s^22p^53s$ (³P₀ or ³P₂). The lifetimes of the two

* Grand Accélérateur National d'Ions Lourds, Caen, France.

metastable states (0.36 ms for ³P₂ and 18 ms for ³P₀ [21]) are long enough for their survival along the path to the collision chamber which is situated six metres away from the ECR source. The beam intensity was of the order of 30 μA.

The incident ion beam is focused on an effusive jet of lithium. Solid lithium is evaporated in an oven which is heated up with a thermocoaxial cable. To avoid heating of the walls of the collision chamber, the furnace is placed in a lining which is cooled by water circulation. The pressure in the collision chamber is of the order of 10⁻⁶ mbar. The lithium jet does not have an influence on the pressure in the collision chamber. The absolute pressure of the lithium jet cannot be measured directly, but the relative pressure is controlled by means of the intensity of the current in the thermocoaxial cable. In order to check that lines attributed to the de-excitation of Ar⁶⁺ and Ar⁵⁺ excited ions correspond actually to double and triple electron captures and not to two or three successive single electron captures, we supposed that the intensities of the lines attributed to single collisions were linear with the pressure (cf. Fig. 1) and then checked that lines intensities corresponding to Ar⁶⁺ and Ar⁵⁺ ions were also linear with the pressure. We also verified that the mean free path of the Ar⁸⁺ incident ion beam large were enough in order that the one-electron capture from the background gas was not possible. Indeed, since the $q \rightarrow q - 1$ cross section for Ar⁸⁺ colliding on H₂, which is a fair assumption for capture from the background gas, is 5.5×10^{-15} cm² [22], the mean free path is of the order of 75 m.

The emitted photons were observed at right angles to the directions of the incident beam and of the lithium jet. They were analysed with a normal incident grating spectrometer of 700 mm focal length (Sopra 700) which contains a grating of 1200 grooves/mm blazed for 750 nm in the first order. A photon counting system was used to detect the emitted photons. This photon counting system consisted of a photomultiplier (Hamamatsu R106) and a microcomputer. Overlapping grating orders are selected by recording four spectra for each set of experimental parameters (incident ion charge, pressure in the Li jet). Three spectra were recorded in the 200–420 nm wavelength range: one without filter, one with a UG5 Schott filter to select lines emitted between 230 and 410 nm and one with a WG305 Schott filter to select lines with wavelengths greater than 305 nm. The fourth spectrum was recorded in the 420–600 nm wavelength range with a GG420 Schott filter to select wavelengths greater than

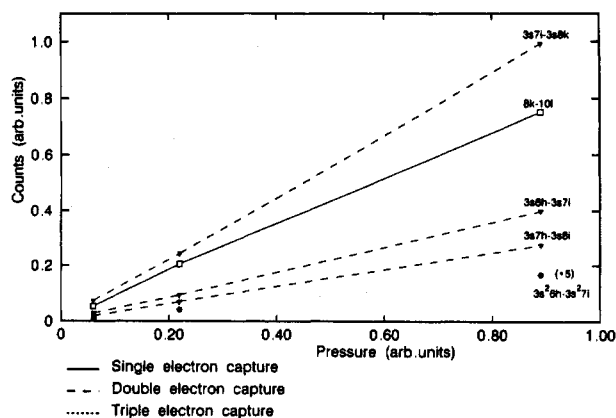


Fig. 1. Evolution of the line intensities with the lithium pressure

Table I. Observed wavelengths of Li I and Li II lines in the 120 keV Ar⁸⁺-Li collisions

Transition	Wavelength (nm)
2s-2p	670.76
2s-3p	323.26
2s-4p	274.13
2p-4s	497.20
2p-3d	610.37
2p-4d	460.29
1s3d-1s4f	467.19

420 nm. Spectra were generally recorded with 0.4 mm wide spectrometer slits and an incremental step of about 0.02 nm per channel in the fourth order. The spectral resolution is then of 0.12 nm in the fourth order. Figure 2 shows the typical spectra obtained. The uncertainty is of ± 0.02 nm in the fourth order (0.03 nm in the third order, 0.04 nm in the second order).

A standard mercury lamp spectrum and some well-known lines emitted by the lithium target published by the National Bureau of Standards [23] were used to determine a specific wavelength calibration curve.

Emission cross sections of the emitted lines were determined to calculate the corresponding excitation cross sections. This requires the calibration of the lines intensities and the determination of the spectroscopic response of the optical device. The absolute calibration of the line intensities has been obtained by recording the spectra for 60 keV C⁴⁺-Li collisions and by using the excitation cross sections for C³⁺(nℓ) determined by Dijkkamp *et al.* [7]. The response of our detection system takes into account the theoretical grating efficiency and the phototube response function given by the manufacturer. This theoretical response is then fitted with well-known lines of C IV. Calibration for Ar⁸⁺-Li collisions is finally obtained by taking into account the ratios of the incident ion beam intensities, the projectile charge states and the target pressures for Ar⁸⁺-Li and C⁴⁺-Li collisions.

We observed seven lines corresponding to Li I and Li II transitions (cf. Table I). As already mentioned, we used them to determine the exact wavelengths in each spectrum.

The photon emission cross sections associated with the lines are presented in Table II. Emission cross sections of lithium lines were also determined. The relative uncertainties are estimated to be $\pm 30\%$ for the greatest lines. They are sufficiently large to take into account polarization effects of the detection that we have not considered.

3. Spectral analysis

3.1. Single electron capture lines

3.1.1. Lines identification. Spectroscopic results. The spectra contain four types of lines: those due to single, double and triple captures and those due to excitation of the target. The single electron capture lines associated with the Ar⁸⁺-Li collisions are not expected to be observed in Ar⁷⁺-Li collisions, so that we recorded the spectra corresponding to Ar⁷⁺-Li collisions. By comparing the spectra registered with the two systems Ar⁸⁺-Li and Ar⁷⁺-Li, we selected single electron capture lines.

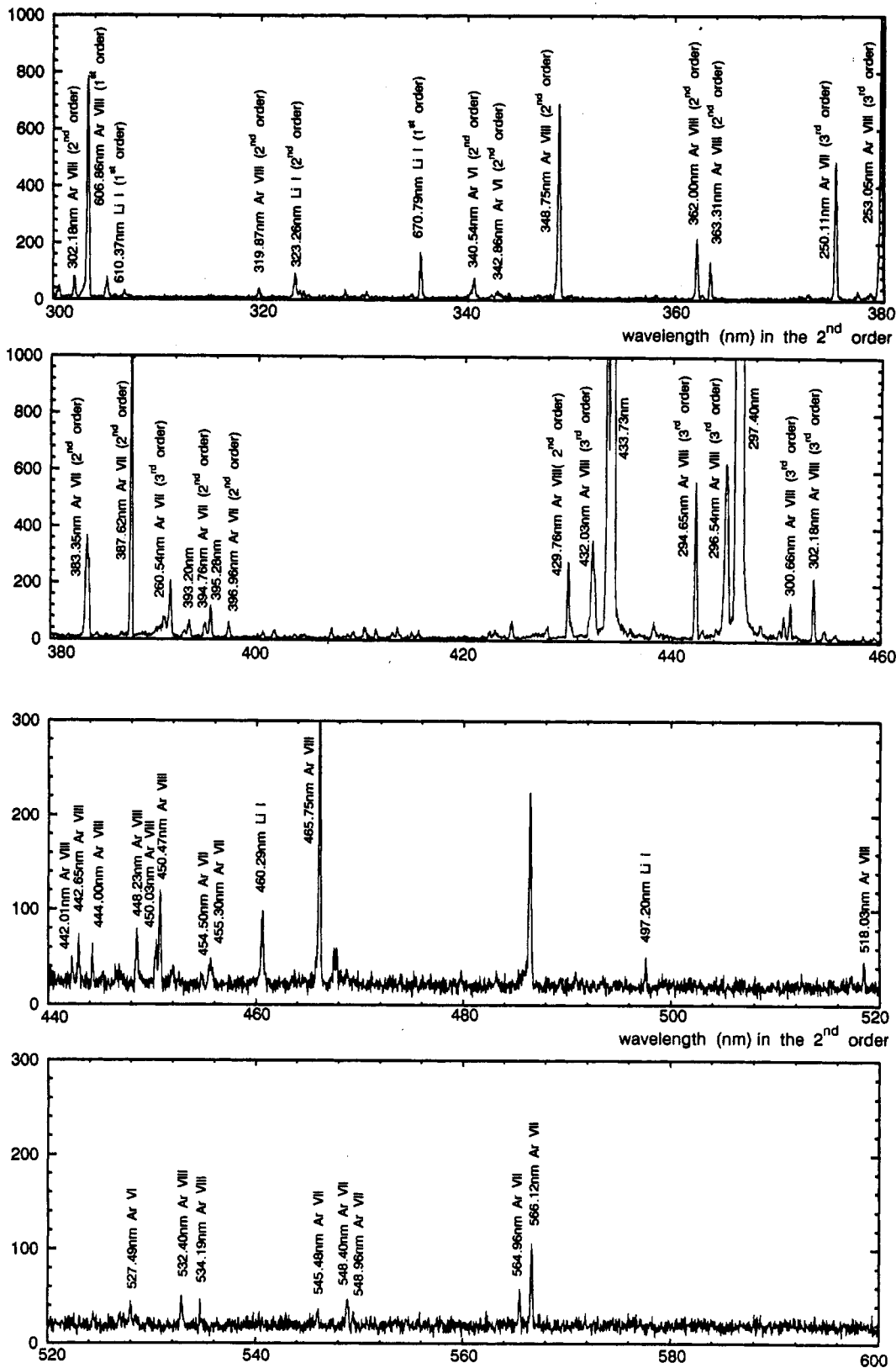


Fig. 2. Spectra of $\text{Ar}^{8+}\text{-Li}$ without filter in the 300–460 nm wavelength range and with a GG420 Schott filter in the 440–600 nm wavelength range

Simple models of single electron capture were used to provide estimates of the states predominantly populated during the collision. The classical barrier model of Ryufuku *et al.* [24] as well as the model of Niehaus [11] predict that the $2s$ electron of the lithium atom is preferentially captured into an $n=9$ orbital. Lines corresponding to transitions $n\ell-n'\ell'$ in Ar VIII with $\Delta n=1$ and 2 are expected to be observed in the 200–600 nm wavelength range. There were

no experimental data concerning these transitions except those between states of large angular momenta already observed by Martin *et al.* [6] and Boduch *et al.* [5]. In order to identify the observed lines, we therefore needed theoretical data. They have been obtained from HFR calculations performed using the Cowan code [15]. Such calculations predict both wavelengths and associated oscillator strengths. The corresponding identifications are described in

Table II. Observed lines in the 200–600 nm wavelength range and their associated emission cross sections ($\Delta\sigma/\sigma$ is of the order of 30%)

Wavelength in air (nm)	Emission cross section (10^{-16} cm ²)	Wavelength in air (nm)	Emission cross section (10^{-16} cm ²)	Wavelength in air (nm)	Emission cross section (10^{-16} cm ²)
228.97 ± 0.03	<0.05	340.82 ± 0.04	<0.05	444.00 ± 0.04	0.11
230.17 ± 0.03	0.06	342.86 ± 0.04	0.17	448.23 ± 0.04	0.10
241.71 ± 0.03	0.12	343.05 ± 0.04	0.07	450.03 ± 0.04	0.10
247.82 ± 0.03	0.07	343.93 ± 0.04	0.05	450.47 ± 0.04	0.20
250.11 ± 0.03	2.51	348.76 ± 0.04	1.59	454.50 ± 0.04	<0.03
251.55 ± 0.03	0.15	361.76 ± 0.04	<0.05	455.30 ± 0.04	<0.03
253.05 ± 0.03	5.33	362.00 ± 0.04	0.44	460.29 ± 0.04	0.19
260.54 ± 0.03	0.24	363.31 ± 0.04	0.23	465.75 ± 0.04	0.90
267.56 ± 0.03	0.15	383.35 ± 0.04	0.72	467.19 ± 0.04	<0.03
271.26 ± 0.03	0.17	385.82 ± 0.04	<0.05	497.20 ± 0.04	0.09
274.13 ± 0.03	<0.05	387.62 ± 0.04	2.72	516.79 ± 0.04	<0.03
282.83 ± 0.03	0.24	388.58 ± 0.04	<0.05	518.03 ± 0.04	0.07
294.65 ± 0.03	1.85	392.73 ± 0.04	<0.05	523.94 ± 0.04	<0.03
296.54 ± 0.03	2.20	393.20 ± 0.04	0.13	527.49 ± 0.04	<0.03
297.18 ± 0.03	9.55	394.76 ± 0.04	0.12	523.40 ± 0.04	0.14
297.46 ± 0.03 ¹	93.6	395.28 ± 0.04	0.24	534.20 ± 0.04	0.06
300.66 ± 0.03	0.35	396.96 ± 0.04	0.6	545.48 ± 0.04	<0.03
302.18 ± 0.03	0.68	410.08 ± 0.04	0.8	548.40 ± 0.04	0.05
305.31 ± 0.03	0.05	429.76 ± 0.04	0.63	548.96 ± 0.04	<0.03
319.87 ± 0.04	0.09	432.03 ± 0.04	0.81	564.96 ± 0.04	0.07
323.26 ± 0.04	0.24	433.54 ± 0.04	4.76	566.12 ± 0.04	0.22
329.77 ± 0.04	0.05	433.92 ± 0.04 ²	77.5	606.86 ± 0.08	4.44
330.20 ± 0.04	0.07	438.02 ± 0.04	0.14	610.37 ± 0.08	0.36
340.26 ± 0.04	0.07	442.01 ± 0.04	<0.05	670.76 ± 0.08	1.22
340.54 ± 0.04	0.19	442.65 ± 0.04	0.07		

¹ High resolution: 297.44 ± 0.01 nm; 297.50 ± 0.01 nm.

² High resolution: 433.89 ± 0.01 nm; 433.98 ± 0.01 nm.

Tables III(a), III(b) and III(c). Only light emitted from states of large and low angular momenta is observed. It corresponds to $\Delta\ell = 1$ transitions ($n' > n$) for transitions involving large values of ℓ and $\Delta\ell = -1$ for transitions involving low values of ℓ . These observations confirm the evolution of the calculated gf values which are strong for $\Delta\ell = 1$ when ℓ is large and which are weak when ℓ is small; for the $\Delta\ell = -1$ transitions gf values are weak when ℓ is large and strong when ℓ is small.

The 465.75 nm line can be attributed to either the $8f-9d$ transition or to the $10m-12n$ transition. On the one hand, this transition has already been observed in Ar⁸⁺-Cs collisions [25] and has been identified as the $10m-12n$ transition; on the other hand, to each $n\ell-n'\ell'$ ($\ell = n-1$ and $\ell' = n'-1$) Rydberg transition in Ar VIII corresponds an $n\ell-n'\ell'$ Rydberg transition in Kr VIII at wavelengths which are nearly the same. As we performed experiments for Kr⁸⁺-Li collisions and as we observed a line at 466.79 nm, we can affirm that this line corresponds to the $10m-12n$ transition.

The wavelengths of the lines due to transitions between states of large angular momenta are very close and in the first spectra the resolution was not great enough to separate the lines. We have then obtained two recorded spectra using narrower spectrometer slits: 0.2 and 0.05 nm and an increase in data acquisition time (cf. Fig. 3). Wavelengths determined in such a manner are those indicated in Tables III(a) and III(b). In these spectra, there are lines which can be attributed to single electron capture by metastable Ar⁸⁺ ions. The intensity of the line corresponding to the $2p^53s(^3P)7i-2p^53s(^3P)8k$ is about 5% of that corresponding to the

$2p^6(^1S)7i-2p^6(^1S)8k$. We do not know the autoionization rate of $2p^53s(^3P)8k$, but all the quartet states and one of the three doublet states born of this configuration are radiative states, we can therefore assume that the incident ion beam contains at least 5% of metastable Ar⁸⁺ ions. For the transition $8k-9l$, the optical resolution was not sufficient to separate the $2p^53s(^3P)8k-2p^53s(^3P)9l$ from the $2p^68k-2p^69l$ transition.

It is noteworthy that we have also identified the two strongest lines of the multiplet corresponding to the $4d-4f$ transitions. Although the well-known $\Delta n = 0$ $5s-5p$ and $5p-5d$ transition [5] lie in our wavelength range, we did not observe them. It is not surprising to observe light emission from the $4f$ configuration since it is strongly populated by

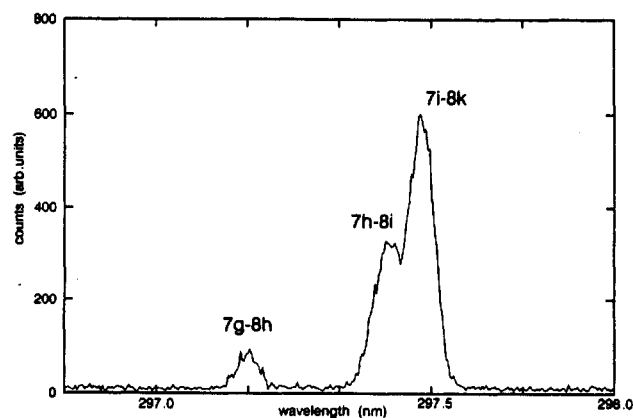


Fig. 3. High resolution spectrum for the Ar⁸⁺-Li system in the 297–298 nm wavelength range

Table III(a). Predicted wavelengths and their associated oscillator strengths and observed $\Delta n = 1$ $7l-8l'$ transitions of Ar VIII due to single electron capture in the 120 keV $Ar^{8+}-Li$ collision

$\Delta n = 1$ transitions in Ar VIII	calc λ (nm) in vacuum	gf	exp λ (nm) in air	$\Delta n = 1$ transitions in Ar VIII	calc λ (nm) in vacuum	gf	exp λ (nm) in air
$7s^2S_{1/2}-8p^2P_{1/2}$	211.82	0.081	—	$7g^2G_{7/2}-8h^2H_{9/2}$	296.62	11.050	297.18
$7s^2S_{1/2}-8p^2P_{3/2}$	211.36	0.162	—	$7g^2G_{9/2}-8h^2H_{9/2}$	296.65	0.251	
				$7g^2G_{9/2}-8h^2H_{11/2}$	296.64	13.560	
$7p^2P_{1/2}-8d^2D_{3/2}$	216.87	0.000	—	$7g^2G_{7/2}-8f^2F_{5/2}$	299.35	0.306	—
$7p^2P_{3/2}-8d^2D_{3/2}$	217.60	0.000	—	$7g^2G_{7/2}-8f^2F_{7/2}$	299.32	0.011	
$7p^2P_{3/2}-8d^2D_{5/2}$	217.54	0.000	—	$7g^2G_{9/2}-8f^2F_{7/2}$	299.35	0.397	
$7p^2P_{1/2}-8s^2S_{1/2}$	301.19	0.000	300.66	$7h^2H_{9/2}-8i^2I_{11/2}$	297.46	18.036	297.44*
$7p^2P_{3/2}-8s^2S_{1/2}$	302.60	0.000	302.18	$7h^2H_{11/2}-8i^2I_{11/2}$	297.48	0.277	
				$7h^2H_{11/2}-8i^2I_{13/2}$	297.47	21.365	
$7d^2D_{3/2}-8f^2F_{5/2}$	268.38	2.097	267.56	$7h^2H_{11/2}-8g^2G_{9/2}$	298.31	0.175	—
$7d^2D_{5/2}-8f^2F_{5/2}$	268.52	0.150					
$7d^2D_{5/2}-8f^2F_{7/2}$	268.49	2.994					
$7d^2D_{3/2}-8p^2P_{1/2}$	363.14	1.476	363.31	$7i^2I_{11/2}-8k^2K_{13/2}$	297.65	28.078	297.50*
$7d^2D_{3/2}-8p^2P_{3/2}$	361.81	0.295	361.76	$7i^2I_{13/2}-8k^2K_{13/2}$	297.67	0.312	
$7d^2D_{5/2}-8p^2P_{3/2}$	362.06	2.664	362.00	$7i^2I_{13/2}-8k^2K_{15/2}$	297.66	32.444	
$7f^2F_{5/2}-8g^2G_{7/2}$	294.31	6.246	294.65	$7i^2I_{11/2}-8h^2H_{9/2}$	297.84	0.065	—
$7f^2F_{7/2}-8g^2G_{7/2}$	294.36	0.231					
$7f^2F_{7/2}-8g^2G_{9/2}$	294.34	8.096					
$7f^2F_{5/2}-8d^2D_{3/2}$	318.55	0.755	319.87	$7i^2I_{11/2}-8h^2H_{11/2}$	297.83	0.001	—
$7f^2F_{5/2}-8d^2D_{5/2}$	318.42	0.054					
$7f^2F_{7/2}-8d^2D_{5/2}$	318.48	1.078					

* Wavelengths obtained with high resolution spectra.
 $2p^53s^3P$ $7i^4K_{17/2}-2p^53s^3P$ $8k^4L_{19/2}$ calc $\lambda = 297.04$ nm, exp $\lambda = 296.54$ nm.

Table III(b). Predicted wavelengths and their associated oscillator strengths and observed $\Delta n = 1$ $8l-9l'$ transitions of Ar VIII due to single electron capture in the 120 keV $Ar^{8+}-Li$ collision

$\Delta n = 1$ transitions in Ar VIII	calc λ (nm) in vacuum	gf	exp λ (nm) in air	$\Delta n = 1$ transitions in Ar VIII	calc λ (nm) in vacuum	gf	exp λ (nm) in air
$8s^2S_{1/2}-9p^2P_{1/2}$	316.12	0.085	—	$8g^2G_{7/2}-9f^2F_{5/2}$	436.74	0.464	—
$8s^2S_{1/2}-9p^2P_{3/2}$	315.42	0.170	—	$8g^2G_{7/2}-9f^2F_{7/2}$	436.69	0.017	
				$8g^2G_{9/2}-9f^2F_{7/2}$	436.73	0.601	
$8p^2P_{1/2}-9d^2D_{3/2}$	320.56	0.097	—	$8h^2H_{9/2}-9i^2I_{11/2}$	433.82	16.820	4.33.54
$8p^2P_{3/2}-9d^2D_{3/2}$	321.60	0.019	—	$8h^2H_{11/2}-9i^2I_{11/2}$	433.86	0.259	
$8p^2P_{3/2}-9d^2D_{5/2}$	321.51	0.175	—	$8h^2H_{11/2}-9i^2I_{13/2}$	433.84	19.924	
$8p^2P_{1/2}-9s^2S_{1/2}$	449.02	0.817	448.23	$8h^2H_{9/2}-9g^2G_{7/2}$	435.13	0.320	—
$8p^2P_{3/2}-9s^2S_{1/2}$	451.07	1.627	450.47	$8h^2H_{9/2}-9g^2G_{9/2}$	435.10	0.007	
				$8h^2H_{11/2}-9g^2G_{9/2}$	435.13	0.392	
$8d^2D_{3/2}-9f^2F_{5/2}$	392.43	2.061	392.73	$8i^2I_{11/2}-9k^2K_{13/2}$	434.12	25.478	433.89*
$8d^2D_{5/2}-9f^2F_{5/2}$	392.63	0.147					
$8d^2D_{5/2}-9f^2F_{7/2}$	392.58	2.943					
$8d^2D_{3/2}-9p^2P_{1/2}$	534.07	1.796	534.20	$8i^2I_{13/2}-9k^2K_{13/2}$	434.16	0.283	—
$8d^2D_{3/2}-9p^2P_{3/2}$	532.07	0.361	—	$8i^2I_{13/2}-9k^2K_{15/2}$	434.16	29.440	
$8d^2D_{5/2}-9p^2P_{3/2}$	532.44	3.242	532.40	$8i^2I_{11/2}-9h^2H_{9/2}$	434.46	0.181	
$8f^2F_{5/2}-9g^2G_{7/2}$	429.38	6.151	429.76	$8i^2I_{11/2}-9h^2H_{11/2}$	434.44	0.003	—
$8f^2F_{7/2}-9g^2G_{7/2}$	429.45	0.228					
$8f^2F_{7/2}-9g^2G_{9/2}$	429.42	7.973					
$8f^2F_{5/2}-9d^2D_{5/2}$	465.71	1.003	—	$8i^2I_{13/2}-9h^2H_{11/2}$	434.46	0.214	433.98*
$8f^2F_{7/2}-9d^2D_{5/2}$	465.52	0.072					
$8f^2F_{7/2}-9d^2D_{7/2}$	465.60	1.433					
$8g^2G_{7/2}-9h^2H_{9/2}$	432.64	10.592	432.03	$8k^2K_{13/2}-9l^2L_{11/2}$	—	—	—
$8g^2G_{9/2}-9h^2H_{9/2}$	432.64	0.241					
$8g^2G_{9/2}-9h^2H_{11/2}$	432.66	12.999					
				$8k^2K_{13/2}-9l^2L_{11/2}$	—	—	—
				$8k^2K_{13/2}-9l^2L_{11/2}$	—	—	
				$8k^2K_{13/2}-9l^2L_{11/2}$	—	—	
				$8k^2K_{13/2}-9i^2I_{11/2}$	434.23	0.067	—
				$8k^2K_{13/2}-9i^2I_{11/2}$	434.22	0.001	
				$8k^2K_{13/2}-9i^2I_{11/2}$	434.23	0.078	

* High resolution.
 $2p^53s^3P$ $7i^4K_{17/2}-2p^53s^3P$ $8k^4L_{19/2}$, calc $\lambda = 433.99$ nm.

Table III(c). Other observed transitions in Ar VIII due to single electron capture in the 120 keV Ar⁸⁺-Li collisions

Transitions in Ar VIII	calc λ (nm) in vacuum	exp λ (nm) in air
$\Delta n = 0$		
$4d^2D_{3/2}-4f^2F_{5/2}$	517.4	516.79
$4d^2D_{5/2}-4f^2F_{5/2}$	520.1	—
$4d^2D_{5/2}-4f^2F_{7/2}$	519.3	518.03
$\Delta n = 1$		
$9h-10i$	606.5	606.86
$9i-10k$	606.9	
$9k-10l$	—	
$9l-10m$	—	
$\Delta n = 2$		
$8f-10g$	251.4	251.55
$8g-10h$	252.6	253.05
$8h-10i$	253.0	
$8i-10k$	253.1	
$8k-10l$	—	
$9g-11h$	348.2	348.76
$9h-11i$	348.7	
$9i-11k$	348.8	
$9k-11l$	—	
$9l-11m$	—	
$10k-12i$	466.0	465.75

 Table III(d). Unidentified single electron capture lines in the Ar⁸⁺-Li 120 keV collisions

Wavelengths (nm)	
282.83	442.65
438.02	444.00
442.01	450.03

cascade effect through the de-excitation of $n\ell$ states with $\ell = \ell_{\max}$ in Ar VIII. Six lines due to single electron capture have not been identified [Table III(d)].

Interesting information about fine structure splittings of the $7p^2P$, $7d^2D$ and $8p^2P$ terms have been deduced from the present identifications (cf. Table IV). They are in good accord with estimates.

3.1.2. One-electron capture cross sections. Another aspect concerning the single electron capture is linked to the production rate of the excited configurations. In order to calculate the cross sections for electron capture into the 8ℓ and the 9ℓ sublevels from the photon emission cross sections indicated in Table II, we have to know branching ratios. We can deduce them from gf values given by HFR calculations.

 Table IV. Experimental and theoretical fine structure splittings $\Delta n(n\ell^2L)$ in cm^{-1} of the $7p^2P$, $7d^2D$ and $8p^2P$ terms of Ar VIII

Fine structures	Calculation	Experiment
$\Delta v (7p^2P)^1$	154.7	167.3 ± 8.8
$\Delta v (7d^2D)^2$	19.1	18.3 ± 6.1
$\Delta v (8p^2P)^2_3$	101.2	117.9 ± 6.1 110.9 ± 4.0

¹ From $7p-8s$.

² From $7d-8p$.

³ From $8p-9s$.

The results are reported in Table V. In order to determine $\sigma(9i + 9k + 9l)$ it is necessary to know individual emission cross sections from $9i$, $9k$ and $9l$ or at least their relative values. These last ones have been deduced from spectra with high resolution and we obtain $\sigma_{\text{em}}(8i - 9k)/\sigma_{\text{em}}(8k - 9l) = 0.16$ and $\sigma_{\text{em}}(8h - 9i)/\sigma_{\text{em}}(8i - 9k) = 0.39$. Table V shows that configurations with large values of the orbital quantum number ℓ are strongly populated, and also that states with very low values of ℓ ($\ell = 0$ and $\ell = 1$) are significantly populated. These results can be compared with those obtained with the CTMC method. As in Refs [9] and [10], where details of the CTMC method can be found, we have used model potentials to describe the interactions between the valence electron and the ionic cores Ar⁸⁺ and Li⁺. The analysis form and the parameters of the model potential for the e^- -Ar⁸⁺ interaction are given in Ref. [9]. For the e^- -Li⁺ interaction, we have used the model potential determined by Klapish [26] to fit spectroscopic data:

$$V(r) = -\frac{1}{r} (1 + 2e^{-7.9r} + 10.31re^{-3.898r}).$$

The calculations were performed taking into account atomic energy levels quantum defects of the Ar⁷⁺ ion. In order to insure small statistical errors 10^5 trajectories were used. The CTMC calculations predict that the largest possible values of ℓ are also preferentially populated and that the rate of increase of the cross sections with ℓ depend strongly on n . The $n\ell$ distribution (see Fig. 4) are sharply peaked for n values near the maximum of the n -distribution ($n = 8$ and 9) whereas they become more statistical for n values far from the maximum ($n = 7$ and 10 for example). We also note that,

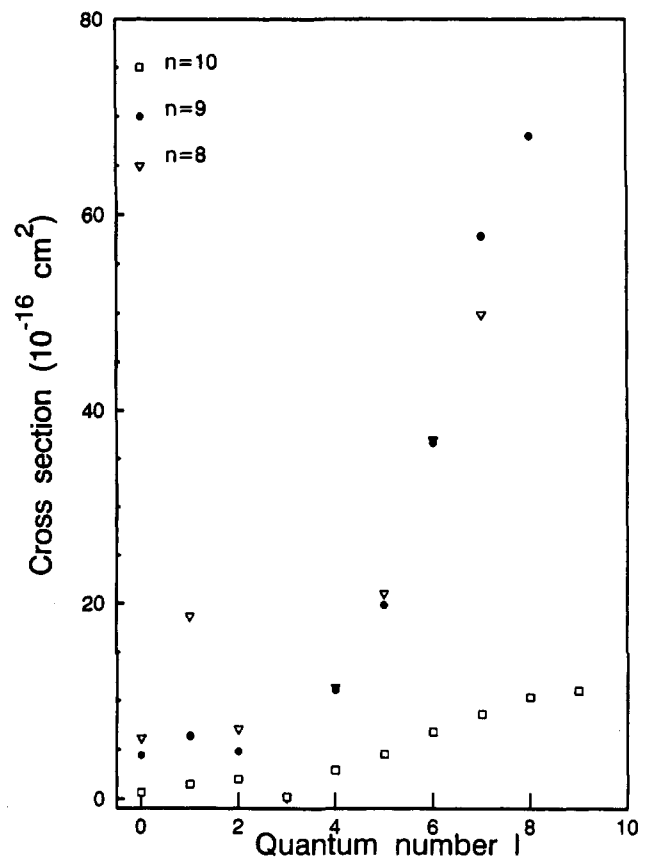


Fig. 4. The calculated n, ℓ distribution for electron capture in Ar⁸⁺-Li(2s) collisions for $n = 8, 9, 10$

Table V. Emission and production cross sections for $n = 8$ and $n = 9$ configurations in Ar VIII populated by single electron capture

Transition in Ar VIII	CTMC emission cross section (10^{-16} cm^2)	Experimental emission cross sections (10^{-16} cm^2)	Configuration in Ar VIII	Experimental production cross section (10^{-15} cm^2)	Calculated production cross section (10^{-15} cm^2)
7p-8s	0.68	1.0	8s	1.1	0.62
7d-8f	0.07	0.15	8p	0.97	1.86
7d-8p	1.49	0.70	8d	0.53	0.71
7f-8g	2.37	1.85	8f	0.33	0.01
7f-8d	0.19	0.09	8g	1.2	1.14
7g-8h	11.44	9.55	8h	5.7	10.8
7h-8i	183.68	93.6	8i		
7i-8k			8k		
8p-9s	0.36	0.30	9s	0.64	0.45
8d-9f	0.01	<0.05	9p	0.39	0.64
8d-9p	0.39	0.20	9d	0	0.49
8f-9g	1.12	0.63	9f	0	0.02
8g-9h	4.23	0.81	9g	0.69	1.11
8h-9i	137.2	82.3	9h	0.52	1.98
8i-9k			9i	9.8	16.23
8k-9l					
4d-4f	0.14	0.08	9k		
9h-10i	27.72	4.4	9l		
9i-10k					
9k-10l					
9l-10m					
8f-10g	0.29	0.15			
8g-10h	11.34	5.33			
8h-10i					
8i-10k					
8k-10l					
9g-11h	3.17	1.59			
9h-11i					
9l-11k					
9k-11l					
9l-11m					

in agreement with the experimental results, the CTMC calculations show that for $n = 8$ and 9 , states with low angular momenta ($\ell = 0, 1, 2$) are produced. Similar results were also obtained from CTMC calculations in the case of Ar^{8+} -Cs(6s) collisions [9], in good agreement with the observations of Martin *et al.* [16, 25] to predict that states of large values of ℓ are preferentially populated. However, in the experiments of Martin *et al.*, no emission from states with low values of ℓ were observed. We can suppose it was only due to technical reasons since it is clear that the predictions of the CTMC calculations are confirmed by our experimental results. Previous CTMC calculations [9] for N^{5+} + Cs(6s) and Ar^{8+} + Cs(6s) collisions have shown a structure in the $n\ell$ distributions more pronounced for Ar^{8+} projectiles than for N^{5+} projectiles. Moreover, recent CTMC calculations for O^{8+} + Li collisions have not found this structure. Therefore, it seems that the structure is due to a core-projectile effect.

The $n\ell$ electron-capture cross sections calculated with the CTMC method are also reported in Table V, and are seen to be in fair agreement with the experimental results. The CTMC calculations give a total cross section of $3.6 \times 10^{-14} \text{ cm}^2$ compared with the experimental value of $2.3 \times 10^{-14} \text{ cm}^2$ for the electron capture into the $n = 8$ and 9 levels preferentially populated. The CTMC calculations give a total overall electron-capture cross section of $5.1 \times 10^{-14} \text{ cm}^2$.

Photon-emission cross sections have also been calculated from the CTMC results. They are reported in Table V. For the $8 \rightarrow 7$ and $9 \rightarrow 8$ transitions, the CTMC results give cross sections of $2.0 \times 10^{-14} \text{ cm}^2$ and $1.44 \times 10^{-14} \text{ cm}^2$ respectively, compared with the experimental values of $1.09 \times 10^{-14} \text{ cm}^2$ and $0.84 \times 10^{-14} \text{ cm}^2$. Note that the experimental value for the $9 \rightarrow 8$ transitions is in close agreement with the experimental data of Wolfrum *et al.* [8] for the similar Ne^{8+} + Li collision system. In view of the present comparisons between CTMC results and experimental data, and also those made recently for C^{6+} , O^{8+} + Li collisions [10], we can conclude that the CTMC method is suitable to predict $n\ell$ single electron capture cross sections for collisions between multiply charged ions and alkali-metal atom targets. For these collisions, the target electron is captured into final states with large values of n , and the one-electron capture process is well described by classical models.

3.2. Double electron capture lines

3.2.1. Determination of the configurations likely to be produced by double electron capture. Before the analysis of double electron capture lines, we tried to determine the configurations likely to be produced. Several kinds of processes may be involved.

The first one is a two-step process: the Li 2s electron and one of the two Li 1s electrons are transferred successively.

For such a process, the model of Niehaus [11] (independent particle model) predicts that the configurations $3p8\ell$ and $3d5\ell$ in Ar VII are predominantly produced. These states are autoionizing states so that they cannot be detected by photon spectroscopy.

The second process that can occur is a one step process involving electron-electron interaction. Following Stolterfoht [27], the energy diagrams presented in Figs 5(a) and 5(b) can give a schematic picture of this process. These diagrams show the orbital energies of the $(\text{Ar}^*-\text{Li})^{8+}$ system vs. the inter-nuclear distance R . The active electrons occupy the $\text{Li}(2s)$ and the $\text{Li}(1s)$ orbitals in the incident channel. If a resonant condition is created at the crossing point $R = R_c$ where the energy of the incident channel ($\text{Ar}^{8+}-\text{Li}$) equals the energy of the outgoing channel ($\text{Ar}^{6+} + \text{Li}^{2+}$), the two electrons can be transferred either into the $3s$ and $n\ell$ orbitals [Fig. 5(a)] or 4ℓ and $4\ell'$ [Fig. 5(b)] (autoexcitation [27]). For instance, for $3s8\ell$ configurations, $R_c = 4.5$ a.u., the resonant conditions being fulfilled, these configurations may therefore be produced by this process. This kind of transfer is referred to as correlated double capture (CDC) [13, 28-30].

Another process called photon stabilized double capture (SDC) in which Rydberg states can be fed from autoionizing states initially populated was proposed by Bachau *et al.* [14]. This mechanism is based on post-collisional effects. The $3d5\ell$ and $3p8\ell$ configurations which may be produced (Niehaus) are not far above the ionization limit (≈ 0.4 a.u.), and, with the influence of the Coulomb field of receding Li^+ ion, these autoionizing states may be stabilized. Configuration interaction can then feed $3sn\ell$ Rydberg states. This process is schematized in Fig. 5(c).

In our case, the $3sn\ell$ configurations in Ar VII may therefore be produced either by CDC [27] or by SDC process.

3.2.2. Line identification. Observed lines corresponding to $3sn\ell-3sn'\ell'$ Rydberg transitions are indicated in Tables VI(a)-VI(b). They have been identified using experimental data from Boduch *et al.* [5] and/or HFR calculations. It was found that these lines correspond to transitions between states of large angular momenta. It is pointed out that these lines are also observed as single electron capture lines in spectra associated with the $\text{Ar}^{7+}-\text{Li}$ collisions. Using the fact that the pressure of the target and at least its variation can be controlled by monitoring the intensities of the single electron capture lines, we can confirm from Fig. 1 that the observed $3sn\ell-3sn'\ell'$ transitions depend linearly on the target pressure and thus correspond to double electron capture lines.

Because of the complexity of the electronic structure of the Ar^{6+} ion, we have not systematically calculated production cross sections for states populated by double electron capture. Nevertheless, for the $3s8k$ configuration which is most likely produced by double electron capture, we can verify from emission cross sections that the corresponding production cross section is of the order of $7 \times 10^{-16} \text{ cm}^2$. Comparison with calculations by means of the Niehaus model suggests that the configurations $3sn\ell$ ($n = 7, 8, 9$) in Ar VII cannot be produced by a two step process. Hence, it is expected that in such collisions, electron-electron interaction through CDC or SDC plays an important role [13, 14, 27, 30].

Several lines indicated in Table VI(c) and quoted as double electron capture lines have not yet been identified. Some of them are strong and have already been observed as

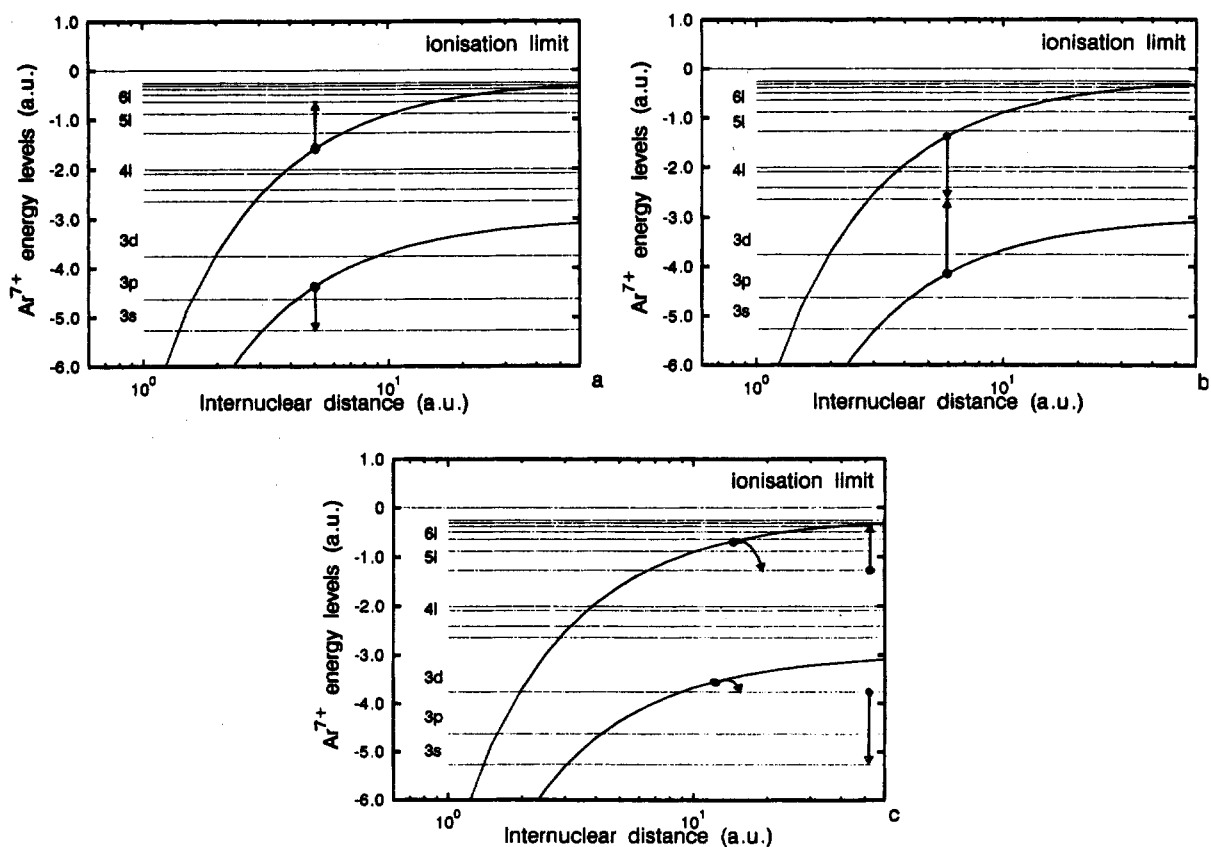


Fig. 5. Schematic illustration of the orbital electron energies for the system $(\text{Ar}-\text{Li})^{8+}$. Double electron capture processes

Table VI(a). Calculated wavelengths and observed $\Delta n = 1$ transitions in Ar VII due to double electron capture in the 120 keV Ar⁸⁺-Li collisions

$\Delta n = 1$ transitions in Ar VII	calc. λ (nm) in vacuum	exp. λ (nm) in air
3s6f ¹ F ₃ -3s7g ¹ G ₄	247.69	247.82 ± 0.03
3s6f ³ F ₄ -3s7g ³ G ₅	241.54	241.71 ± 0.03
3s6g ¹ G ₄ -3s7h ¹ H ₅	249.29	250.11 ± 0.03
3s6g ³ G ₅ -3s7h ³ H ₆	248.04	247.82 ± 0.03
3s6h ¹ H ₅ -3s7i ¹ I ₆	250.59	250.11 ± 0.03
3s6h ³ H ₆ -3s7i ³ I ₇	250.54	
3s7g ¹ G ₄ -3s8h ¹ H ₅	384.94	383.35 ± 0.04 (1)
3s7g ³ G ₅ -3s8h ³ H ₆	382.80	
3s7h ¹ H ₅ -3s8i ¹ I ₆	385.80	
7s7h ³ H ₆ -3s8i ³ I ₇	385.67	
3s7i ¹ I ₆ -3s8k ¹ K ₇	388.17	387.62 ± 0.04
3s7i ³ I ₇ -3s8k ³ K ₈	388.17	
3s8i-3s9k	565.8	565.96 ± 0.04
3s8k-3s9l	—	566.12 ± 0.04

Table VI(b). Calculated wavelengths and observed $\Delta n = 2$ transitions in Ar VII due to double electron capture in the 120 keV Ar⁸⁺-Li collisions

$\Delta n = 2$ transitions in Ar VII	calc. λ (nm) in vacuum	exp. λ (nm) in air
3s7h-3s9i	229.6	228.97 ± 0.03
3s7i-3s9k	230.5	230.17 ± 0.03
3s8i-3s10k	330.2	329.77 ± 0.04
3s8k-3s10l	—	330.20 ± 0.04
3s9i-3s11k	454.9	—
3s9k-3s11l	—	454.50 ± 0.04
3s9l-3s11m	—	455.30 ± 0.04

Table VI(c). Unidentified double electron capture lines in 120 keV Ar⁸⁺-Li collisions

Wavelengths (nm)	
260.54*	395.28*
271.26	396.96*
305.31	410.08
385.82*	545.48*
388.58	548.40*
393.20*	548.96
394.76*	

* Double electron capture lines already observed by Boduch *et al.* [5].

double electron capture lines by Boduch *et al.* in Ar⁸⁺-He collisions [5]. They have also been observed in Ar⁷⁺-Li collisions as single electron capture lines (in such a case, they are probably due to a transfer excitation mechanism). We suggest that they correspond to the emission from states belonging to configurations $3pn\ell$ ($n = 4$ or 5) or $3d4\ell$. These configurations may be produced by an uncorrelated two-step process or by correlated double capture. HFR calculations involving configurations interactions have been performed but it is difficult to find identifications which are consistent with the theoretical predictions. This is probably due to the fact that it is difficult to take correctly into account all the configurations interactions in these calcu-

Table VII. Observed $\Delta n = 1$ transitions in Ar VI due to triple electron capture in the 120 keV Ar⁸⁺-Li collisions

exp. λ (nm) in air	Transition in Ar VI
340.26	3s3p(³ P)6h ² H _{9/2} -3s3p(³ P)7i ² I _{11/2}
340.54	{ 3s ² (¹ S)6h ² H-3s ² (¹ S)7i ² I 3s3p(³ P)6h ² H _{11/2} -3s3p(³ P)7i ² I _{13/2}
340.82	3s3p(³ P)6h ² H _{11/2} -3s3p(³ P)7i ² I _{11/2}
342.86	3s3p(³ P)6h ² H-3s3p(³ P)7i ² K
343.05	—
343.93	3s3p(³ P)6h ² G-3s3p(³ P)7i ² H
523.94	3s ² (¹ S)7h ² H-3s ² (¹ S)8i ² I
527.49	3s ² (¹ S)7i ² I-3s ² (¹ S)8k ² K

lations. We will study this problem in more detail in the future.

3.3. Triple electron capture lines

3.3.1. *Determination of the configurations produced by triple electron capture.* Several kinds of processes may be involved. Firstly, three electrons of the target may be captured successively. For this three-step process, we can assert that the configurations $3\ell 3\ell' n\ell''$ ($n = 7, 8$) in Ar⁵⁺ are produced [Fig. 6(a)].

Secondly, we consider a two step process where two electrons are captured simultaneously and the third one in an additional step. This second process can produce two kinds of configurations: if the 2s electron of lithium is captured alone, configurations $3s3dn\ell$ ($n = 7, 8$) can be produced [Fig. 6(b)]; if one of the 1s electron is captured alone, $3s3pn\ell$ ($n = 7, 8$) can be produced [Fig. 6(c)].

3.3.2. *Line identification.* Observed lines corresponding to $3s^2n\ell-3s^2n'\ell'$ and $3s3p(^1P$ or $^3P)n\ell-3s3p(^1P$ or $^3P)n'\ell'$ Rydberg transitions are indicated in Table VII. They have been identified using experimental data [18] and/or HFR calculations. These lines were also observed as single electron capture lines in spectra associated with Ar⁶⁺-Li collisions. Indeed, since Ar⁶⁺ ions are either in their ground states or in a metastable state (³P), single electron capture can produce $3s^2n\ell$ or $3s3pn\ell$ ($n = 6, 7$) configurations in Ar VI. We verified that the intensities of the lines due to Ar⁵⁺ ions are linear with the lithium vapour pressure (Fig. 1). The observed transitions $3s^2n\ell-3s^2n'\ell'$ correspond actually to triple electron capture lines.

4. Conclusion

We performed a detailed spectroscopic work in the range of near UV and visible light for the collision system 120 keV Ar⁸⁺-Li. The analysis provides information about the atomic structure of Ar⁷⁺, Ar⁶⁺ and Ar⁵⁺ ions as well as about collisions mechanisms involved in single, double and triple electron captures. The spectroscopic analysis has allowed the identification of numerous radiative transitions. Many lines are observed and interpreted for the first time. The experimental transition energies are found to be in excellent agreement with HFR calculations.

The results for single-electron capture confirm the validity of the classical over barrier models. Fine structure components of $7p^2P$, $7d^2D$ and $8p^2P$ were deduced. The production cross sections for $n = 8$ and $n = 9$ states are evaluated from emission cross sections. They indicate that

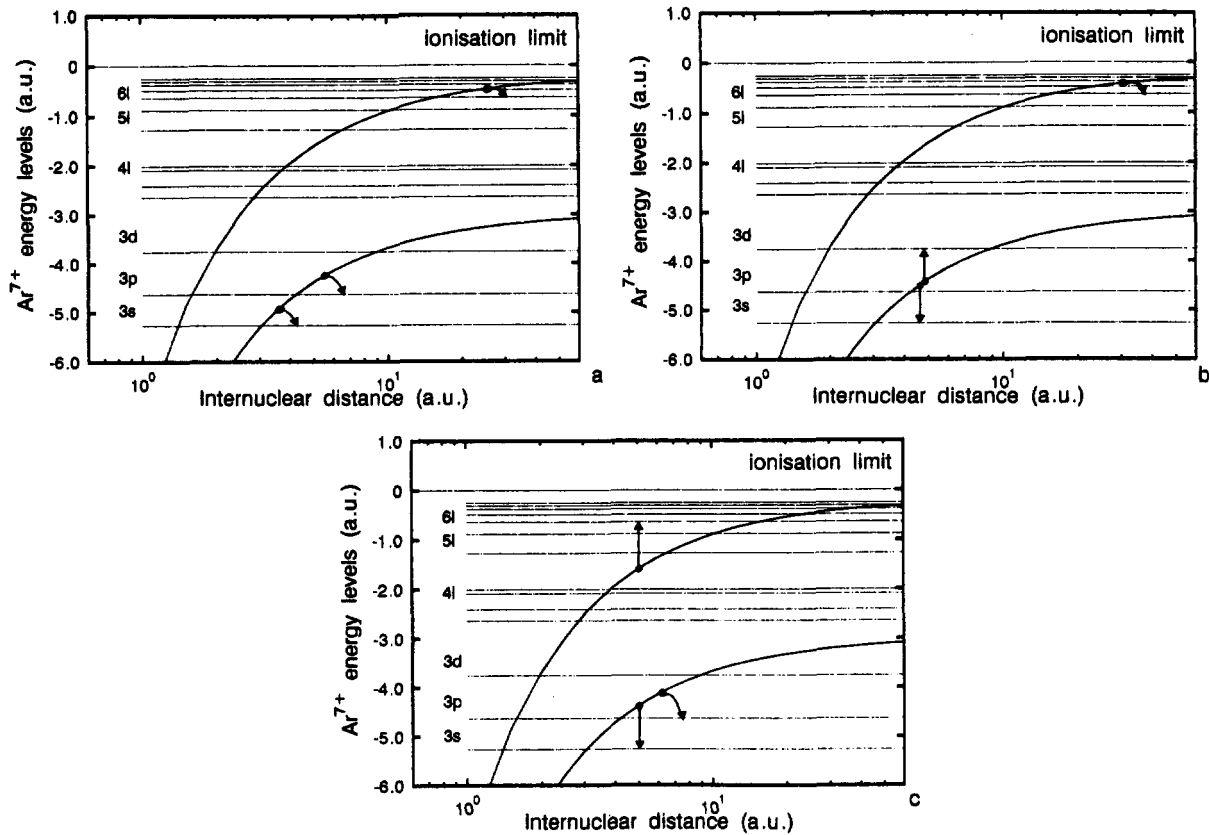


Fig. 6. Schematic illustration of the orbital electron energies for the system (Ar-Li)⁸⁺. Triple electron capture processes

only states of large angular momenta and states of low angular momenta are populated in good agreement with CTMC calculations.

For double and triple electron capture, three kinds of processes have been considered. In the first one, dielectronic interactions are neglected and the electrons are attracted successively by the nucleus. In the other two processes (CDC or SDC), dielectronic interaction is supposed to play an important role. We can hence explain the strong emissions due to Rydberg transitions in Ar VII and Ar VI and assume that configurations $3pn\ell$ in Ar VII are produced with high probability.

Acknowledgements

It is a pleasure to acknowledge the staff of the test bench at GANIL for their efficient support. We would also like to thank R. D. Cowan for his generous help in implementing the codes used here. Part of this work was supported by the SERC through a grant to use the Cray XMP of the Rutherford Appleton Laboratory.

References

- Melan, E. P. and Wegner, G., *Astrophys. J.* **289**, L31 (1985).
- Rosen, M. D., Hagelstein, P. L., Matthews, D. L., Campbell, E. M., Hazi, A. U., Whitten, B. L., MacGowan, B., Turner, R. E. and Lee, R. W., *Phys. Rev. Lett.* **54**, L106 (1985).
- Post, D. E., Grisham, L. R. and Fonck, R. J., *Physical. Scripta* **3**, L31 (1983).
- Boduch, P., Chantepie, M., Hennecart, D., Husson, X., Kucal, H., Lecler, D. and Lesteven-Vaisse, I., *J. Phys. B: At. Mol. Phys.* **22**, L377 (1989).
- Boduch, P., Chantepie, M., Druetta, M., Fawcett, B., Hennecart, D., Husson, X., Kucal, H., Lecler, D., Stolterfoht, N. and Wilson, M., *Physica Scripta* **45**, 203 (1992).
- Martin, S., Do Cao, G., Salmoun, A., Bouchama, T., Denis, A., Andra, J., Désesquelles, J. and Druetta, M., *Physics Letters* **A133**, 239 (1988).
- Dijkkamp, D., Brazuk, A., Drentje, A. G., de Heer, F. J. and Winter, H., *J. Phys. B: At. Mol. Phys.* **17**, 4371 (1984).
- Wolftrum, E., Hoekstra, R., de Heer, F. J., Morgenstern, R. and Winter, H., *J. Phys. B: At. Mol. Phys.* **25**, 2597 (1992).
- Pascale, J., Olson, R. E. and Reinhold, C. O., *Phys. Rev.* **A42**, 5305 (1990).
- Olson, R. E., Pascale, J. and Hoekstra, R., *J. Phys. B: At. Mol. Phys.* **25**, 4231 (1992).
- Niehaus, A., *J. Phys. B: At. Mol. Phys.* **19**, 2925 (1986).
- Stolterfoht, N., Haveneur, C. C., Phaneuf, R. A., Swenson, J. K., Shafroth, S. M. and Meyer, F. W., *Phys. Rev. Lett.* **57**, 74 (1986).
- Stolterfoht, N., Sommer, K., Swenson, J. K., Haveneur, C. C. and Meyer, F. W., *Phys. Rev.* **A42**, 5396 (1990).
- Bachau, H., Roncin, P. and Harel, C., *J. Phys. B: At. Mol. Phys.*, **25**, L109 (1992).
- Cowan, R. D., "The Theory of Atomic and Spectra" (University of California Press, Berkeley 1981).
- Martin, S., Salmoun, A., Ouerdane, Y., Druetta, M., Désesquelles, J. and Denis, A., *Phys. Rev. Lett.* **62**, 2112 (1989).
- Martin, S., Denis, A., Désesquelles, J. and Ouerdane, Y., *Physical Review* **A42**, 6564 (1990).
- Boduch, P., Chantepie, M., Druetta, M., Hennecart, D., Husson, X., Jacquet, E., Lecler, D. and Wilson, M., *Physica Scripta*, **47**, 24 (1993).
- Albrines, R. and Percival, I. C., *Phys. Soc.* **88**, 861 (1966).
- Olson, R. E. and Salop, A., *Phys. Rev.* **A16**, 531 (1977).
- Bhatia, A. K., Feldman, U. and Seely, J. F., *At. Data: Nucl. Data Tables* **32**, 435 (1985).
- Crandall, D. H., Phaneuf, R. A. and Meyer, F. W., *Phys. Rev.* **A22**, 379 (1980).
- "Atomic Transition Probabilities" (Vol. 1) (U.S. Department of Commerce, National Bureau of Standards, Washington 1966).
- Ryufuku, H., Sasaki, K. and Watanabe, T., *Phys. Rev.* **A21**, 745 (1980).
- Martin, S., Denis, A., Ouerdane, Y., Carré, M., Buchet-Poulizac, M. C. and Désesquelles, J., *Phys. Rev.* **A46**, 1316 (1992).
- Klapish, M., Thesis, Université Paris-Sud, Orsay, unpublished (1969).
- Stolterfoht, N., *Physica Scripta* **42**, 192 (1990).
- Stolterfoht, N., *Nucl. Instr. Meth.* **B53**, 477 (1991).
- Frémont, F., Sommer, K., Lecler, D., Hicham, S., Boduch, P., Husson, X. and Stolterfoht, N., *Phys. Rev.* **A46**, 217 (1992).
- Mann, R. and Schulte, H., *Z. Phys. D - Atoms, Molecules and Clusters* **4**, 343 (1987).